Spatial Asymmetry in Tactile Sensor Skin Deformation Aids Perception of Edge Orientation During Haptic Exploration

Ruben D. Ponce Wong, *Member, IEEE* , Randall B. Hellman, *Student Member, IEEE* , and Veronica J. Santos, *Member, IEEE*

Abstract—Upper-limb amputees rely primarily on visual feedback when using their prostheses to interact with others or objects in their environment. A constant reliance upon visual feedback can be mentally exhausting and does not suffice for many activities when line-of-sight is unavailable. Upper-limb amputees could greatly benefit from the ability to perceive edges, one of the most salient features of 3D shape, through touch alone. We present an approach for estimating edge orientation with respect to an artificial fingertip through haptic exploration using a multimodal tactile sensor on a robot hand. Key parameters from the tactile signals for each of four exploratory procedures were used as inputs to a support vector regression model. Edge orientation angles ranging from −90 to 90 degrees were estimated with an 85-input model having an R^2 of 0.99 and RMS error of 5.08 degrees. Electrode impedance signals provided the most useful inputs by encoding spatially asymmetric skin deformation across the entire fingertip. Interestingly, sensor regions that were not in direct contact with the stimulus provided particularly useful information. Methods described here could pave the way for semi-autonomous capabilities in prosthetic or robotic hands during haptic exploration, especially when visual feedback is unavailable.

Index Terms—Active touch, exploratory procedures, haptic perception, prosthetic, robotic

1 Introduction

The intimate connection between an amputee and his or her upper-limb prosthesis brings together two complex systems that speak different languages at different timescales. Communication delays inherent to human-machine systems result from the necessary translation between the biological and artificial systems for both afferent and efferent signals [1]. The cognitive burden on an amputee can be minimized by making the prosthesis more intuitive to use and minimizing the details that the amputee must consider in light of such delays. Subtle details of control include determining which of the multitude of joints to actuate, when and how hard to grasp an object, and how to adjust fingertip forces to maintain stability during object grasp and tool use.

Invasive techniques such as targeted muscle reinnervation [2], peripheral nerve stimulation [3], and intracortical microstimulation [4], [5], [6] hold the promise of bringing a conscious perception of tactile feedback to the user and increasing the number of channels with which a user can intuitively control a high degree-of-freedom (DOF) prosthesis (see [7] for a nice review of anthropomorphic prosthetic hands). Even when such techniques become clinically viable and commonplace, amputees may still not be able to respond quickly enough through the human-machine interface to counter unexpected perturbations or perform tasks requiring quick dexterous adjustments.

Amputees could benefit from the use of a "sense-think-act" circuit [8] within the prosthesis itself that automatically addresses ms-to-ms details of finger-object actions, and buys time for cognitive processing and generation of a voluntary response. Complex behaviors could also be semi-automated so that the user could focus on high level decisions so long as the semi-automation is context-appropriate, reliable, and does not alienate the user.

Currently, amputees who use commercially available upper-limb prostheses rely solely upon visual feedback when physically interacting with others or objects in their environment [1]. Visual feedback can provide preliminary information that can be used to pre-shape grasp [9] and plan digit placement [10]. However, visual feedback alone cannot provide all essential information for successful physical hand-object interactions. This is especially true when object scenes are cluttered, pre-planned digit placement is poor or erroneously executed, digits are occluded by the grasped object, or the hand-object interaction is completely out of view. Everyday examples include searching for a light switch in the dark, wrapping a belt around oneself, or reaching for a cellphone in one's pocket.

Performance of activities of daily living with a prosthesis requires extensive concentration which can be mentally taxing, especially for a bilateral amputee who cannot compensate for a missing limb with an unimpaired limb. Reliance upon visual feedback alone is especially challenging because many activities of daily living do not afford a complete line-of-sight or require precise control of fingertip forces whose effects are unseen. A survey of amputees who use transradial electric-powered prostheses reiterated that

• *The authors are with the Mechanical and Aerospace Engineering program, Arizona State University, 501 E. Tyler Mall, ECG 301, MC 6106, Tempe, AZ 85287-6106. E-mail: {rponcewo, rhellman, veronica.santos}@asu.edu.*

Manuscript received 4 May 2013; revised 20 Sept. 2013; accepted 8 Oct. 2013. Date of publication 20 Oct. 2013; date of current version 18 June 2014.
Recommended for acceptance by A. Frisoli, M. O'Malley, D. Campolo, and K. Sienko.
For information on obtaining reprints of this article, please send e-mail to: reprints@ieee.org, and reference the Digital Object Identifier below.
Digital Object Identifier no. 10.1109/TOH.2013.56

amputees would prefer that less visual attention be required to perform functions [11]. This desirable feature was ranked third out of 17 choices, behind basic kinematic preferences for fingers that can bend and a thumb that can move out to the side.

A study on three-dimensional (3D) haptic shape perception investigated the influence of object features such as curvature, aspect ratio, and edges on the ability of unimpaired subjects to quickly and accurately identify objects through touch alone [12]. Subjects were allowed to use a variety of "exploratory procedures" (EPs) [13] in order to extract object properties. The study concluded that edges and vertices were the most salient local features of 3D shape and that haptic searches were performed efficiently when the target object had edges [12], [14].

Given the usefulness of edges in human studies on shape perception, it could be worthwhile to develop artificial capabilities for edge perception in artificial systems, such as prosthetic or robotic hands. While enclosure could be used for estimating global shape, enclosure has yet to be used for edge perception by artificial hands, possibly due to limitations in tactile sensing technology. Rather, enclosure has been used to simplify the grasp planning problem, particularly with underactuated hand designs (e.g., [15], [16]). Contour-following has been demonstrated for industrial applications, but simultaneous force and vision sensing were required [17], [18]. Edge detection has been demonstrated for artificial fingers using touch alone, but the typical approach has been to use raster-like patterns of static contact with the object to build a composite "tactile image" [19], [20], [21], [22]. Such raster-like patterns do not reflect common strategies used by humans, such as dynamic hand and finger movements for surface tracing and contour-following [12], [23].

Whether conveying a sense of touch to an amputee or making a split-second semi-autonomous decision on the amputee's behalf, a prosthesis must have an ability to relate finger-object interactions to a hand-centric reference frame. The objective of this work was to enable an artificial hand to estimate the orientation of a salient local feature (edge) of an object with respect to a fingertip reference frame during haptic exploration. The ability to perceive edge orientation with respect to the fingertip through active touch could enable task-appropriate manipulations of an object and complex exploratory procedures such as contour-following [13] in the absence of visual feedback.

2 Methods

2.1 Apparatus

2.1.1 Robot Testbed

The robot testbed consists of a seven-degree-of-freedom Barrett Whole Arm Manipulator (WAM) and BarrettHand (Barrett Technology, Cambridge, MA) in which the middle digit has been outfitted with a BioTac sensor (SynTouch, Los Angeles, CA) (Fig. 1). The BioTac enables simultaneous measurement of multiple tactile sensing modalities that mimic slow- and fast-adapting mechanoreceptors in the human fingertip. This multimodal tactile sensor has been used to identify material type [24], compliance [25], and texture [26], to relate haptic adjectives to objects [27], and to identify objects [28]. The sensor consists of a fingertip-shaped rigid core that houses an array of 19 electrodes, a pressure sensor, and a thermistor [29]. An elastomeric skin, patterned externally with fingerprint-like ridges, surrounds the rigid core [26]. A weakly conductive fluid injected between the core and elastic skin serves as the fluidic mechanotransduction medium.

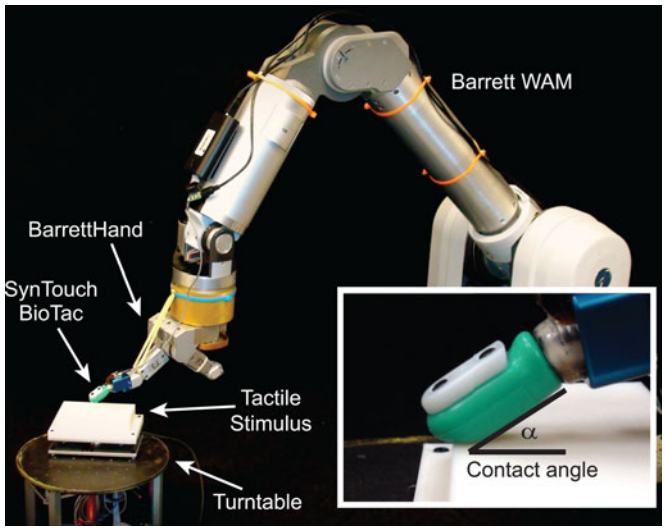

Fig. 1. The Barrett WAM, BarrettHand, and BioTac were used to explore edge stimuli presented at random orientations with respect to the fingertip reference frame by a motor-driven turntable.

While the mechanotransduction mechanisms differ from those of the human fingertip, the electrodes of the BioTac serve as low spatial resolution proxies for Merkel's disks, slow-adapting cutaneous mechanoreceptors in the human finger that respond to local, low-frequency skin deformations [30]. When low-pass filtered, the pressure sensor output serves as a proxy for Ruffini's corpuscles, slow-adapting mechanoreceptors that respond remotely to static forces [31]. When high-pass filtered, the pressure sensor output mimics the dynamic range (but not the spatial resolution) of Meissner's and Paciniian corpuscles, fast-adapting mechanoreceptors in the human fingertip that respond to high frequency vibrations and mechanical transients [26], [32].

Per manufacturer specifications, the tactile sensor employed sampling rates of 100 Hz for overall internal fluid pressure and electrode impedance (for each of the 19 electrodes in the spatial array), and 2,200 Hz for vibratory signals [31]. Thus, for each 10 ms batch of data, we recorded 19 signals from the spatial array associated with elastomeric skin deformation relative to the sensor's rigid core, one sample of overall internal fluid pressure, and 22 samples of fluid vibration data. Since we were primarily interested in the effect of mechanical stimuli during dynamic fingertip movements, temperature measurements were not used in this work.

2.1.2 Tactile Stimuli

We hypothesized that edge orientation angle θ would be encoded in the tactile data. For instance, exploratory movements perpendicular to an edge might produce more vibrations than movements aligned with an edge.

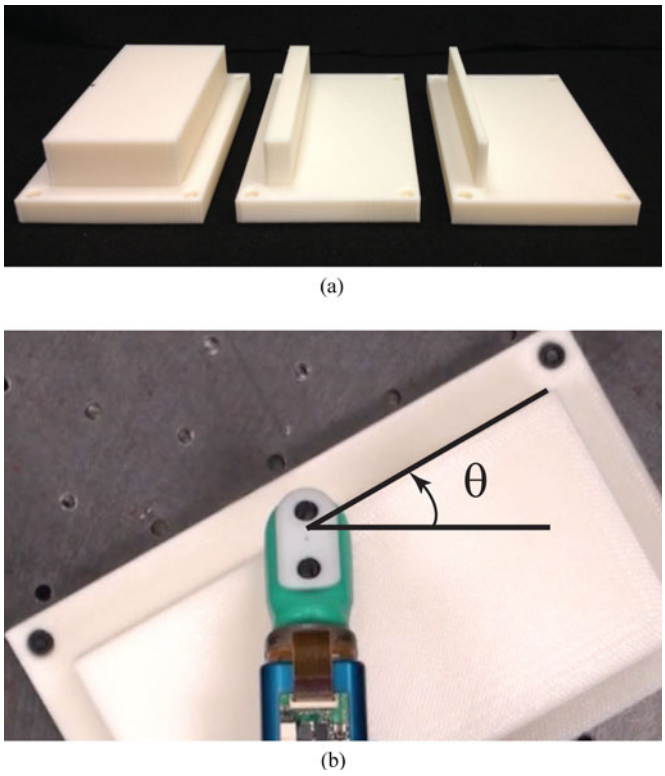

Fig. 2. (a) Edge stimuli of three different widths were presented at (b) different orientation angles θ with respect to a fingertip ref. frame.

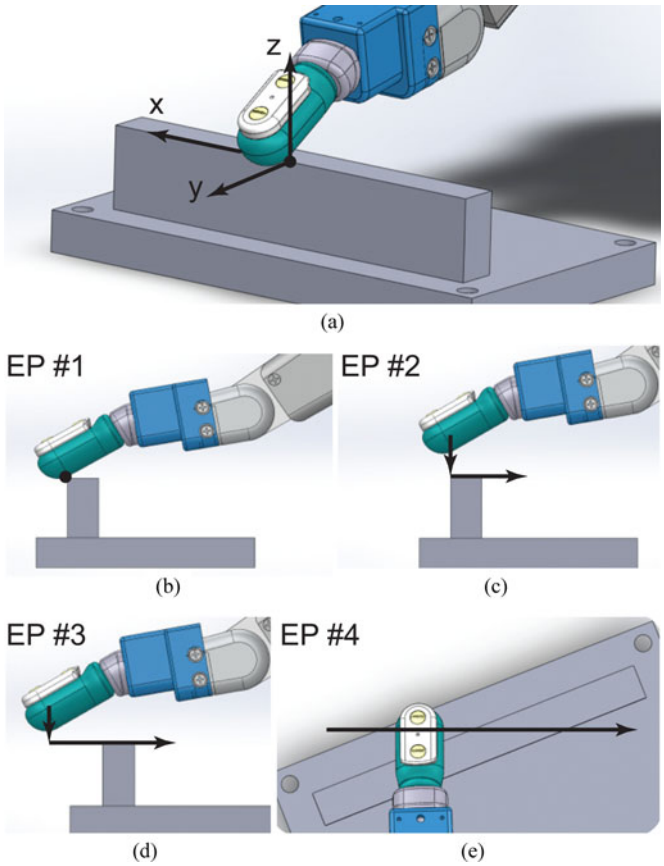

Fig. 3. (a) During each exploratory procedure, the WAM maintained a constant BioTac contact angle relative to the horizontal *x*-*y* plane. (b) EP #1: static contact, (c) EP #2: distal to proximal stroke with an approach normal to the stimulus surface, (d) EP #3: distal to proximal stroke with an approach tangential to the stimulus surface, and (e) EP #4: radial to ulnar stroke. The reader is referred to the supplementary video, to view the implementation of the four EPs.

In order to develop a generalizable support vector regression (SVR) model capable of estimating edge orientation regardless of surface width, we collected data for three different surface widths. Three 2 cm-tall, 3D printed edge stimuli were used: a 5 cm-wide "broad surface," a 1 cm-wide "thick bar," and a 0.4 cm-wide "thin bar," (Fig. 2a). Each stimulus was rigidly attached to a 6-DOF load cell (ATI Nano-17), which was attached to a steel turntable. The load cell was used to record the nominal force of the fingertip during contact with the stimulus.

A DC motor (Maxon Precision Motors, Inc., EC-max 30) and motor controller (Maxon EPOS2 24/5) were used to orient edges in the horizontal plane at angles ranging from -90 to 90 degrees (quadrants I and IV) in 1 degree increments in a randomized order. Experimental results with angles in quadrants II and III were presumed to be symmetric about the longitudinal axis of the artificial finger and were not investigated. Edge orientation angles were measured relative to a positive x-axis (0 degrees) pointing in the ulnar direction of a right-hand index finger (Figs. 2b and 3a).

For each trial, the motor rotated the edge to a prescribed angle with a resolution of 1/2,000 counts per revolution, or 0.18 degrees. Just prior to BioTac contact with the stimulus, a pair of electromagnets were activated, which locked the turntable position and triggered the temporary powering down of the DC motor to minimize electromagnetic noise pollution of the 6-DOF load cell data. Edge orientation was randomized in order to minimize possible effects of skin wear or other latent variables on the SVR model.

2.2 Exploratory Procedures

Joint-space control of the WAM was used to prescribe the trajectory of the BioTac fingertip and its orientation using Barrett Technology's internal C++ library ("libbarrett"). The trajectories for the EPs were solved offline in joint space using a custom quaternion-based, pseudo-inverse iterative solver. The joint space trajectories were used as inputs to Barrett's tracker that runs a PID controller for each joint at 500 Hz. The PID gains were initially set by a calibration routine and then tuned by hand to minimize oscillations during contact with the stimulus.

Four specific exploratory procedures were used: 1) static contact, 2) distal to proximal linear stroke along the y-axis with an approach normal to the stimulus surface, 3) distal to proximal linear stroke along the y-axis with an approach tangential to the stimulus surface, and 4) radial to ulnar linear stroke along the x-axis (Fig. 3). A fixed global reference frame was defined directly above the center of the turntable with its origin placed at the contact height of the stimulus and its x-y plane coincident with the stimulus surface. Axes were defined such that radial to ulnar and distal to proximal fingertip motions could be expressed in terms of x- and y-coordinates while fingertip height could be expressed in z-coordinates (Fig. 3a).

The four EPs are shown in Fig. 3 and in the supplementary video, which can be found on the Computer Society Digital Library at http://doi.ieeecomputersociety.org/10.1109/TOH.2013.56, accompanying this work. For EP #1 (Fig. 3b), the fingertip was pressed against the edge of the stimulus with an approach normal to the stimulus surface, at the origin of the global reference frame, at a constant nominal force in the –z direction for a "hold" period of 1.5 sec. For EP #2 (Fig. 3c), the fingertip approached the edge along the z-axis (normal to the surface), made contact with the edge, and then swept across the edge in the –y direction. For EP #3 (Fig. 3d), the fingertip approached the edge from a location distal to the edge along the y-axis (tangential to the surface), and then swept across the edge in the –y direction. For EP #4 (Fig. 3e), the fingertip swept across the stimulus in the ulnar direction along the x-axis. However, the nature of the first contact for this EP varied according to edge orientation and surface width. For example, relatively steep negative edge orientations were such that, for the thin and thick bars, the initial contact was tangential to the stimulus surface while, for a broad surface, the initial contact was normal to the stimulus surface. A constant fingertip height was commanded for all four EPs. Details on the commanded fingertip height, stroke trajectory, and contact angle are provided in the following paragraphs.

A linear stroke of constant speed was used to investigate the quality of tactile information gleaned from a simple motion. Scanning speeds were inspired by non-human primate and human subject experiments on sensing and perception of stimulus orientation in which bars and edges were scanned linearly across a passive fingerpad at speeds of 1, 2, 4, and 8 cm/s [33], [34]. EP #2 and #3 fingertip trajectories used velocities of $v_y = -2$ cm/s or -4 cm/s. For EP #2, initial contact always occurred at the origin of the global reference frame (Fig. 3a) and was followed by a 4 cm stroke in the –y direction. Initial contact for EP #3 occurred at different locations along the edge of the stimulus, depending on edge orientation. However, as with EP #2, the stroke trajectory of EP #3 ended at $y = -4$ cm. EP #4 fingertip trajectories used velocities of $v_x = +2$ cm/s or $+4$ cm/s and were 8 cm long (started at $x = -4$ cm and ended at $x = +4$ cm).

For all four EPs, the BioTac was oriented at either a 20 or 30 degree contact angle α with respect to the horizontal x-y plane (Fig. 1). A 30 degree contact angle was prescribed such that the cluster of four electrodes on the flat face of the BioTac (Fig. 4, Cluster 1) would be parallel to the surface to be explored (Figs. 1 and 4). A shallower contact angle of 20 degrees was used to stimulate a wider range of electrodes, particularly on the proximal aspect of the BioTac.

For the 30 degree contact angle, the sensor was swept across each stimulus for all four EPs at one of two constant commanded heights from the stimulus surface ($z = -4$ mm or -6 mm) in order to examine two different nominal contact forces. Fingertip displacements were selected to ensure that the BioTac skin would deform substantially as it swept over each stimulus. A commanded height of $z = -4$ mm only was used for the 20 degree BioTac contact angle since early studies showed that SVR model performance was unaffected by the magnitude of the applied force. The reduced fingertip contact force helped to minimize unnecessary wear of the BioTac skin.

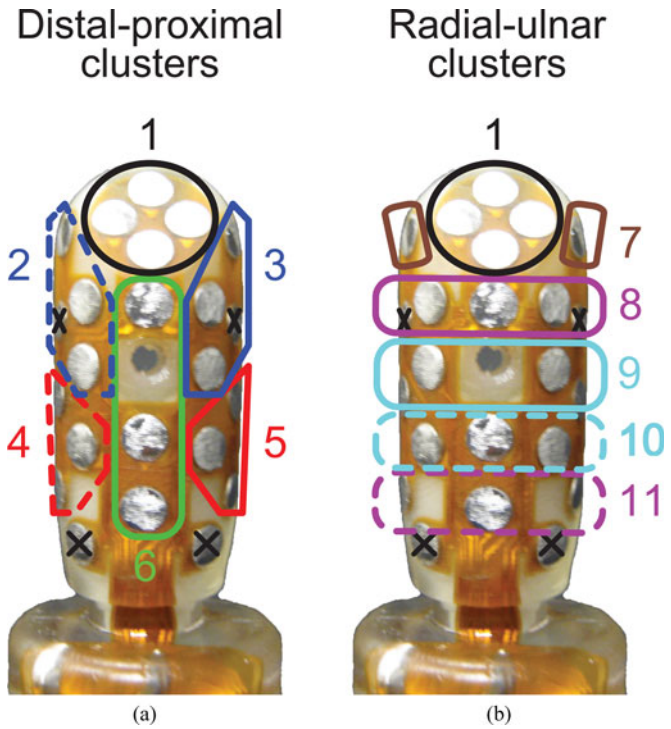

Fig. 4. BioTac electrodes were clustered based on their spatial location on the rigid core (palmar view of a right-hand index finger shown without the skin). Clusters were either oriented along the (a) distal-proximal axis or (b) radial-ulnar axis.

2.3 Processing of Tactile Sensor Data

Similar to the human fingertip, the BioTac is sensitive to sustained (slow) and transient (fast) stimuli. We hypothesized that key information about finger-object interactions would be encoded in both slow and fast tactile signals during different phases of each contact. Thus, different "windows" of tactile data, specific to the exploratory procedure, were used to train the SVR model. Windows were labeled with a "W" followed by the number of the EP, a period, and the number of the window for that particular EP (Table 1). A single window (W1.1) was used for EP #1, six windows (W2.1-W2.6) were used for EP #2, and four windows (W3.1-W3.4 or W4.1-W4.4) were used for each of EP #3 and #4. Windows applied to fast tactile signals (W2.4-W2.6, W3.3, W3.4, W4.3, and W4.4) were truncated versions of windows applied to slow tactile signals. All windows will be described further in the following paragraphs. Fig. 5 shows each window as a shaded bar beneath each tactile data type.

2.3.1 *Overall Fluid Pressure*

For each trial, a threshold of a 3 percent increase from baseline overall fluid pressure was used to determine initial contact and loss of contact. Since the SVR model was to be based on stimuli having different surface widths, contact time was normalized by converting each contact period into a percentage where 0 and 100 percent denoted initial contact and loss of contact, respectively.

For EP #1 (static contact), the middle 30 percent of contact (W1.1) was used to calculate inputs to the SVR model (Fig. 5). It was observed that EP #2 (normal

TABLE 1
SVR Model Input Parameters

Type of info	Input to SVR model	EP #1	EP #2	EP #3	EP #4
Voluntary motion	Scanning speed	---	(1) Single value for entire trial		
Slow tactile signals	Overall fluid pressure	(1) W1.1	(3) W2.1-W2.3	(2) W3.1, W3.2	(2) W4.1, W4.2
	Initial rates of change of overall fluid pressure	---	(1) W2.1	(1) W3.1	(1) W4.1
	Electrode impedance	(6) W1.1 for Clusters 1-6	(18) W2.1-W2.3 for Clusters 1-6	(12) W3.1, W3.2 for Clusters 1-6	(12) W4.1, W4.2 for Clusters 1-6 *or* 1,7-11
	Initial rates of change of electrode impedance	---	(6) W2.1 for Clusters 1-6	(6) W3.1 for Clusters 1-6	(6) W4.1 for Clusters 1-6 *or* 1,7-11
Fast tactile signals	Instant. freq. (of 1st IMF) of vibrations	---	(3) W2.4-W2.6	(2) W3.3, W3.4	(2) W4.3, W4.4

Parenthetical values in red indicate the number of inputs for each type of parameter.

approach, Fig. 3c) generated tactile data that resembled the concatenation of a static contact (as with EP #1) followed by a stroking motion. As a result, data from the stroke with the normal approach were split into three windows: brief static contact (W2.1), first half of the remaining motion (W2.2), and second half of the remaining motion (W2.3). For EP #3 and #4, the data were split into two equal windows of contact (W3.1 and W3.2 for EP #3, W4.1 and W4.2 for EP #4). Windows were selected in order to capture trends during the contact period (sustained values during static contact, dynamics at the start and end of strokes).

A mean overall pressure value was calculated for each window of time (W1.1, W2.1-W2.3, W3.1-W3.2, W4.1-W4.2) for use as inputs to the SVR model. In addition, initial rates of change were provided to the model. Overall fluid pressure data were low-pass filtered with a second order Butterworth filter having a cut-off frequency of 10 Hz prior to numerical differentiation. Mean rates of change were calculated for the first 25 percent of windows W2.1, W3.1, and W4.1 to extract information embedded in the slow tactile signals that might be unique to edge orientation and initial sensor-stimulus contact.

2.3.2 Skin Deformation

In a previous study, a cluster of four electrodes on the fingertip and a lateral electrode enabled estimation of material compliance [25]. Thus, although the BioTac provides independent impedance values for each of 19 electrodes, we used clusters of electrodes defined according to spatial location on the fingertip and oriented along either the distal-proximal axis (Fig. 4a) or the radial-ulnar axis (Fig. 4b).

Mean electrode impedances were calculated for each cluster (for windows W1.1, W2.1-W2.3, W3.1-W3.2, W4.1-W4.2) in order to reduce the number of inputs of the SVR model, problem complexity, and computational expense. As with the overall fluid pressure signals, electrode impedance data were low-pass filtered with a second

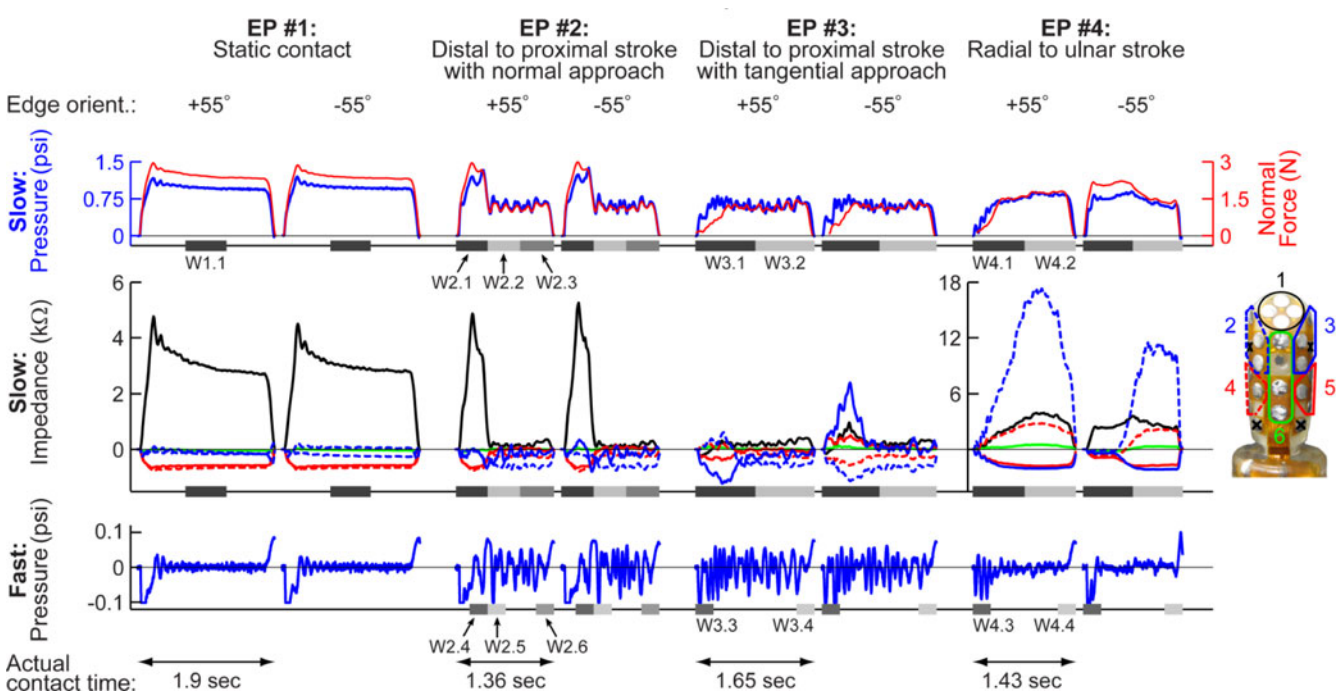

Fig. 5. Representative multimodal tactile data for edge orientations of +55 and –55 degrees for a broad surface, contact angle of 30 degrees, commanded displacement of $z = -4$ mm, and scanning speed of 4 cm/s. Overall fluid pressure (row 1, blue) was used to determine initial contact and loss of contact. Inputs to the SVR model were calculated from windows of time (W1.1-W4.4) that were specific to each exploratory procedure. For each EP, the same windows were used for the two types of slow tactile signals (overall fluid pressure, electrode impedance).

order Butterworth filter having a cut-off frequency of 10 Hz, and mean rates of change for each cluster were calculated for the first 25 percent of windows W2.1, W3.1, and W4.1.

2.3.3 Fluid Vibration

With the exception of EP #1 (static contact), each window of fluid vibration data was analyzed using a Hilbert-Huang Transform (HHT) [35], [36]. Like the Fast Fourier Transform (FFT), the HHT converts data from the time domain to the frequency domain. While HHT is more computationally intensive than FFT, a major advantage is that HHT is applicable to data sets that do not satisfy assumptions of linearity and stationarity [37]. The transient and discontinuous nature of the tactile data generated from a stroke across an edge, for example, makes the HHT preferable for this work.

The HHT process deconstructs the original signal into intrinsic mode functions (IMFs), each of which has its own energy content and frequency spectrum, by applying empirical mode decomposition. The first IMF component contains the highest frequencies of the original signal. The second IMF contains the next highest frequencies, and so on [35], [38].

Hypothesizing that information related to edge orientation would be contained in the high frequency range, we selected the first IMF for extracting input parameters for the SVR model for EP #2, #3, and #4. For EP #2, an attempt was made to capture the dynamics at the start and end of the stroke by defining windows W2.4, W2.5, and W2.6 as the last 250 ms of W2.1, the first 250 ms of W2.2, and the last 250 ms of W2.3, respectively (Fig. 5). For EP #3 and #4, the dynamics at initial contact and loss of contact were investigated. Windows W3.3 and W3.4 were defined as the first 250 ms of W3.1 and the last 250 ms of W3.2, respectively, for EP #3 while W4.3 and W4.4 were defined as the first 250 ms of W4.1 and the last 250 ms of W4.2, respectively, for EP #4. For those cases in which windows W2.4-W2.6, W3.3-W3.4, W4.3-W4.4 may have been shorter than 250 ms in duration, the entire window of data was used. For each of windows W2.4-W2.6, W3.3-W3.4, W4.3-W4.4, the mean instantaneous frequency of the first IMF was used as an input to the SVR model.

2.4 Support Vector Regression Model

A support vector machine is a well-established supervised learning technique for classification and regression, with advantages such as robustness to outliers and convergence to a global minimum [39]. To enhance the practical utility of our work, we elected to develop a support vector regression model that estimates a value from a continuous number line as opposed to a support vector classifier that will simply identify a single class from a limited set of discrete classes selected a priori and which may not generalize to data on which the classifier was never trained. Cross-validation was used to evaluate the effects of and establish model learning parameters. Model performance and effects of user-specified input parameters were assessed using a novel test data set that was not used during the training or building of the model.

We collected two trials of tactile data for each of 181 randomized edge orientations and for each of 18 distinct block conditions (three stimuli surface widths, two contact angles, two scanning speeds, two commanded displacement heights for the 30 degree contact angle and one height for the 20 degree contact angle). Each individual trial consisted of data resulting from all four exploratory procedures. For each block condition, data were split randomly into a training set ($\sim$90 percent of total trials) and test set ($\sim$10 percent of total trials). Ultimately, 5849 trials were used for training an SVR model while 648 trials were saved for testing of the final model. Cross-validation to select learning parameters (kernel function, complexity term) was performed on the training data only.

When building the SVR models using WEKA [40], we considered up to 85 input parameters (Table 1). Besides the tactile signals described previously, scanning speed was used as an input parameter because of the relationships that presumably exist between active fingertip motions (easily quantified for robotic systems) and sensations elicited at the fingertip. Normal contact forces and contact angles were left out of the SVR models as these parameters would depend on the compliance and shape of the object and would likely be unknown in practice.

3 Results

3.1 Tactile Data

For a commanded fingertip height of $z = -4$ mm, the normal contact forces (mean $\pm$ standard dev.) during the middle 30 percent of EP #1 (W1.1) were 1.30 ± 0.46 N and 2.72 ± 0.58 N for the 20 and 30 degree contact angle cases, respectively. For a commanded fingertip height of $z = -6$ mm (30 degree contact angle case only), the normal contact forces were 3.48 ± 0.70 N.

Representative multimodal tactile sensor signals are shown in Fig. 5 for all four EPs for two different edge orientations that are symmetric about the radial-ulnar x-axis: $+55$ and -55 degrees. Baseline (pre-contact) values were subtracted for all tactile signals on a trial-by-trial basis. For each EP, the overall fluid pressure (Fig. 5, row 1, blue) and normal contact force (Fig. 5, row 1, red) increase and decrease as would be expected with initial contact and loss of contact, respectively. The stroking motion of the fingertip results in lower overall fluid pressures (Fig. 5, row 1, W2.2-W2.3, W3.1-W3.2, W4.1-W4.2) and increased fluid vibration amplitudes (Fig. 5, row 3). Interestingly, despite their nearly identical distal to proximal fingertip motions, EP #2 and #3 generated qualitatively different tactile signals due to their different approaches to the stimulus surface (normal or tangential, respectively).

Each of the clusters of electrodes measures skin deformation near a specific region of the BioTac's 3D, curved core. For the distal-proximal clusters (Fig. 4a) whose data are presented in Fig. 5, clusters that were not located along the long axis of symmetry of the sensor (clusters 2-5) displayed an asymmetric response for EP #3. Compression of the skin against the rigid core resulted in an increase in impedance on one side of the finger, such as the radial aspect for a -55 degree orientation. This trend was mirrored by a

TABLE 2
SVR Model Performance Using Different Sets of Inputs

Focus of Comparisons	EP #	# of Inputs	R^2	Mean abs. error (°)	RMS error (°)
Exploratory procedures (using all available input parameters for each EP)	1-4	85	0.991	2.893	5.076
	1	7	0.441	30.719	39.685
	2	32	0.712	18.531	28.409
	3	24	0.960	5.177	10.668
	4	24	0.725	17.338	27.908
	3, 4	47	0.980	3.457	7.511
Removal of scanning speed, overall fluid pressure, and vibration inputs	1-4	66	0.987	3.205	6.114
	3	18	0.931	6.632	14.015
	4	18	0.686	19.258	29.800
Removal of initial rates of change of overall fluid pressure and electrode impedance*	1-4	48	0.858	12.720	19.904
	3	12	0.795	15.892	24.091
Removal of specific distal-proximal clusters (Fig. 4a)*					
- Centerline (Clusters 1, 6) removed	3	12	0.784	16.991	25.093
- Ulnar aspect (Clusters 2, 4) removed	3	12	0.792	16.902	24.102
- Radial aspect (Clusters 3, 5) removed	3	12	0.777	17.679	25.095
Radial-ulnar clusters (Fig. 4b)					
- All available input parameters	4	24	0.709	17.724	28.836
- Electrode impedance values only*	4	18	0.500	26.157	37.353

*Appealing models based on accuracy with respect to the number of input parameters are shown in red. EP #3 and electrode impedance signals provided the most useful inputs for this edge orientation perception task. *With scanning speed, overall fluid pressure, and vibration inputs also removed.*

simultaneous bulging of the skin away from the rigid core and resulted in a decrease in impedance on the other side of the finger, such as the ulnar aspect for the −55 degree orientation (Fig. 5, dashed lines in row 2). For EP #4 (radial to ulnar stroke), shear forces caused a compression of the skin against the rigid core on the ulnar aspect and a bulging of the skin on the radial aspect.

3.2 Model Performance

From cross-validation observations, the kernel function and complexity term of the SVR model were set to a quadratic polynomial and a value of 1, respectively. The low model complexity term minimizes overfitting of the model to the training data. These settings yielded accurate estimations of edge orientation for a variety of EP and input parameter combinations (Table 2).

An SVR model using all 85 inputs took approximately 20 hours to be trained and built on a PC with two Intel Xeon 2 GHz quad core processors. When all 85 inputs were used in the SVR model, a regression of the model estimations on the true edge orientations for the test data set yielded an R^2 of 0.991 (Table 2, Fig. 6). Appealing model options, based on accuracy with respect to the number of input parameters, appear in red in Table 2.

4 Discussion

4.1 Estimation of Edge Orientation

We trained a support vector regression model with data from thousands of interactions with edge stimuli having three different surface widths, at two different contact angles, at two different nominal contact forces, and with two different scanning speeds. Accurate estimations of edge orientation were possible even without providing the SVR model with information on stimulus width, fingertip displacement in the z-direction, or contact angle (Tables 1 and 2). In practice, the only movement-related information one could provide to the SVR model is the known scanning speed of the artificial fingertip.

As shown in Table 2, when comparing SVR models based on different exploratory procedures, most models having R^2 values greater than approximately 0.8 yielded mean absolute and RMS errors that fell within the [2.5, 25] degree range of human perception thresholds

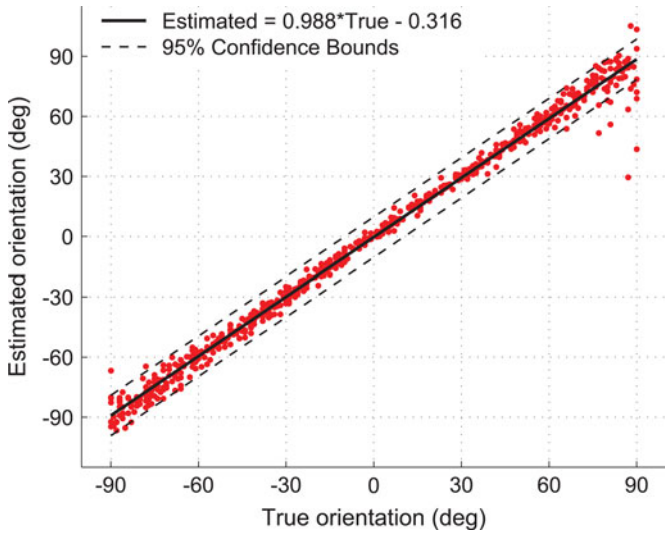

Fig. 6. An SVR model using all 85 inputs performed well on the test data set (648 trials, ~10 percent of total trials, R^2 of 0.99, RMS error of 5.08 degrees), which included various edge orientations, stimulus widths, normal contact forces, contact angles, and scanning speeds.

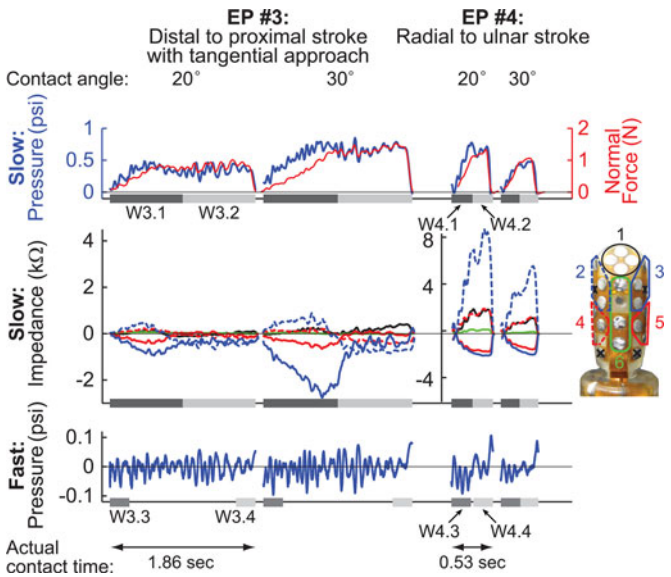

Fig. 7. Representative multimodal tactile data for the 20 and 30 degree contact angles during EP #3 and #4 for a thick bar oriented at +75 degrees, commanded displacement of $z = -4$ mm, and scanning speed of 4 cm/s. Although the 20 degree contact angle resulted in lower normal contact forces than the 30 degree contact angle, the electrode impedance values still captured useful spatiotemporal information related to edge orientation.

for tactile perception of edge and bar orientation [34]. This finding suggests that the accuracy of the SVR model for perception of edge orientation in a plane is comparable to that of humans, so long as appropriate inputs are provided to the regression model.

Model performance was worst when estimating larger magnitude angles (namely, above 55 degrees) regardless of their direction (+ or −) (Fig. 6). One possibility is that there was increased variability in the stroking motions for larger magnitude angles, which would lead to variability in the training data and inaccuracy in model estimations for large angles. For instance, when steep angles were encountered in which the edge was nearly aligned with the long axis of the finger, the BioTac would sometimes move alongside the edge during EP #3 before stroking the top surface of the stimulus.

4.1.1 *Effects of Contact Angle*

The primary effect of reducing the contact angle from 30 to 20 degrees was a dramatic drop in normal contact force, resulting in smaller overall fluid pressure and electrode impedance values. For a commanded fingertip height of $z = -4$ mm, the normal contact forces during the middle 30 percent of EP #1 (W1.1) dropped from 2.72 ± 0.58 N to 1.30 ± 0.46 N.

Our original hypothesis was that a shallower contact angle of 20 degrees might stimulate a wider range of electrodes. However, all else being equal, the 30 degree contact angle produced larger skin deformations and, thus, larger changes in electrode impedance values. Despite the drop in magnitudes across the different tactile data modes for the 20 degree contact angle case, information about edge orientation remained encoded in the tactile data, especially the electrode impedance time histories (Fig. 7).

4.2 Effects of the Exploratory Procedure

Our results show that the exploratory procedure directly affects the trends in the multimodal tactile sensor data (Fig. 5) and that model performance based on the different EPs can vary (Table 2). EP #1 (static contact) provides a sustained period of overall fluid pressure and electrode impedance data (Fig. 5). A comparison of EP #2 and EP #3 quickly reveals how even a subtle difference in approach direction (normal or tangential, respectively) between the two otherwise identical stroking motions can affect the tactile data. For example, there are stark differences in electrode impedance trends for lateral clusters 2-5 between EP #2 (Fig. 5, row 2, W2.1-W2.3) and EP #3 (Fig. 5, row 2, W3.1 and W3.2).

It is hypothesized that skin deformation during initial contact of the BioTac against the stimulus determines how the skin will deform for the remainder of the stroking motion. When the approach to the surface is along the normal direction as with EP #2, the fingertip makes static contact first, which compresses electrode cluster 1 and constrains radial-ulnar pairs of clusters (2-3 and 4-5) to change in concert during initial contact. When the approach is tangential to the surface as with EP #3, the skin is free to deform according to the orientation of the leading edge of the stimulus. As a result, the radial-ulnar pairs of clusters reflect opposite trends in electrode impedance upon contact.

It was observed that electrode impedance values were much larger for EP #4 than for EP #3 (rows 2 of Figs. 5 and 7). This observation may be due to an increase in skin contact area for the radial to ulnar stroke of EP #4 as compared to the distal to proximal stroke of EP #3. Another possibility is that the robot testbed, specifically the basal joint of the fixed middle BarrettHand finger, was less compliant during collisions with edges when the fingertip moved along the x-axis.

When building a model using EP #1 (static contact) only, the R^2 value was 0.441 and mean absolute and RMS errors were 30.72 and 39.69 degrees, respectively (Table 2). When a stroking motion was used, model performance increased substantially (R^2 of 0.712, 0.960, and 0.725 for EP #2, #3, and #4, respectively). In this study, we implemented a static contact (EP #1) with a normal approach. A model based on EP #1 might perform better if a tangential approach were used or if individual electrode impedance data were provided to the model instead of cluster data. EP #3 (distal to proximal stroke with a tangential approach) led to the most accurate model with an R^2 value of 0.96 and mean absolute and RMS errors of 5.18 and 10.67 degrees, respectively (Table 2).

If one chose to use all four EPs in practice, the R^2 value could be as high as 0.99 and the mean absolute and RMS errors could be as low as 2.89 and 5.08 degrees, respectively. However, the tradeoff for such an accurate model is the need to collect tactile data for all exploratory procedures for each trial and the increased complexity of the SVR model (85 inputs). The system designer must assess whether the slight increase in

estimative power is worth the additional exploratory procedures, computational expense of tactile data post-processing, and model complexity (beyond the 24 inputs for EP #3 only).

4.3 Efficient Sets of Model Input Parameters

We built multiple SVR models in order to gauge the usefulness of different EPs and model inputs, and to find efficient sets of inputs (Table 2). As stated previously, EP #3 was found to be the most useful single exploratory procedure (R^2 value of 0.96 and RMS error of 10.67 degrees).

After removing scanning speed, overall fluid pressure, and vibration input parameters, the R^2 value only dropped from 0.991 to 0.987 when all four EPs were considered (removal of 19 input parameters) and from 0.960 to 0.931 when only EP #3 was considered (removal of six input parameters). This finding suggests that the electrode impedance data provide the most useful information for estimating edge orientation. Scanning speed does not seem to be critical since we have already normalized contact time to a percentage during post-processing. Although useful in detecting contact and delineating windows of time, overall fluid pressure does not seem to provide information that is not already included in the impedance signals. The fluid vibration data provided some information about edge orientation magnitude, but not much about direction.

We also investigated the relative importance of spatial location of electrode impedance data. First, distal-proximal clusters of electrodes were considered (Fig. 4a). Focusing on EP #3, the R^2 value for a model without scanning speed, overall fluid pressure, or vibration data dropped from 0.931 to 0.784, 0.792, and 0.777 after removing electrode impedance data from clusters along the centerline (clusters 1 and 6), ulnar aspects (clusters 2 and 4), and radial aspects (clusters 3 and 5), respectively (Table 2). Thus, spatial asymmetry in the skin deformation data appears to be especially important for this task of estimating edge orientation.

4.4 Notable Trends in the Tactile Data

4.4.1 *Usefulness of Spatial Asymmetry in the Tactile Sensor Signals*

For the edge orientation task of this work, it appears that the estimative power of the SVR model is owed primarily to the asymmetry of the slow tactile data (electrode impedance values) with respect to the long axis of the finger. Through both normal and shear forces, electrode impedance increased when the elastomeric skin was compressed against the rigid core of the sensor. Simultaneously, another part of the skin would bulge away from the core. The distal to proximal motion of EP #3 resulted in opposite trends in electrode impedance for clusters on the radial and ulnar aspects of the fingertip (Fig. 4a; solid versus dashed lines in Figs. 5 and 7).

Considering that the radial to ulnar motion of EP #4 might be better represented by clusters specific to the distal and proximal aspects of the fingertip (Fig. 4b), a direct comparison was made between the two different cluster scenarios (Fig. 8). Distal-proximal clusters appear

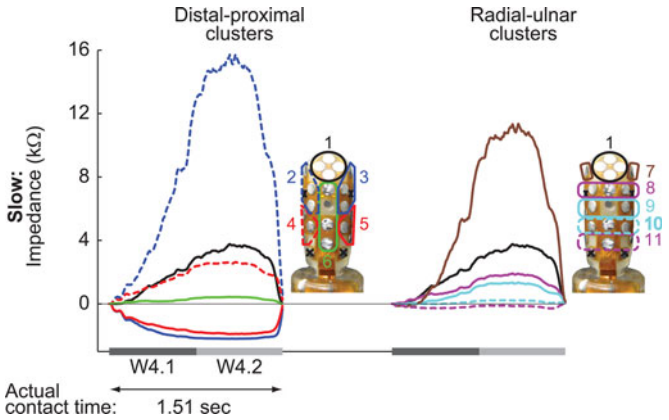

Fig. 8. Representative electrode impedance data for distal-proximal clusters and radial-ulnar clusters. Data are shown for EP #4, a broad surface oriented at $+35$ degrees, a 30 degree contact angle, a commanded displacement of $z = -4$ mm, and scanning speed of 4 cm/s. Distal-proximal clusters appear to better capture skin deformation towards and away from the rigid core.

to better capture bulging of the skin away from the sensor core, as evidenced by relatively large negative electrode impedance values. Radial-ulnar clusters typically yield primarily positive impedance values (Fig. 8). It appears as if the skin compression and bulging effects on the radial and ulnar aspects of the fingertip get nullified mathematically when radial-ulnar clusters are used. Without scanning speed, overall fluid pressure, and vibration input parameters, models with radial-ulnar clusters had an R^2 value of 0.50 and RMS error of 37.4 degrees for EP #4 as compared to models with distal-proximal clusters which had an R^2 value of 0.69 and RMS error of 29.8 degrees (Table 2). These results suggest that clusters that effectively capture skin deformation can be selected independently of the fingertip velocity vector.

4.4.2 *Effects of a Bladder-Type Tactile Sensor Construction*

The richness of the tactile data generated from EP #3 alone highlights the usefulness of simple finger-object interactions and how tactile sensors that make use of deformable skins as part of the mechanotransduction process (e.g., [29], [41], [42], [43]) may yield advantages beyond shock absorption, increased contact area, and tackiness of the grip. A typical robotics approach of mounting rigid, 6-DOF force transducers on artificial fingertips might be straightforward from a traditional modeling and grasp planning perspective [44], but such an approach may be inappropriate for obtaining insight into human finger-object interactions with deformable skin and multimodal tactile sensing capabilities. Analytical modeling of the BioTac sensor and physical interactions with objects was considered, but it was concluded that our research questions were more tractable with robot experiments than the creation of a complex multi-physics model that would have to address deformation of an elastic skin, incompressible fluid, electrostatics, and fluid vibration.

Interestingly, the tactile data that enabled accurate estimation of edge orientation were generated by regions of the tactile sensor that were not in direct contact with the stimulus. Electrode clusters 2-5 (Fig. 4) were not always compressed by the finger-object interaction. The free surface of the skin was able to bulge away from the rigid core of the sensor. This finding has interesting consequences for the development of tactile sensing systems for artificial hands. Traditionally, for reasons of cost and simplicity, a designer might place tactile sensor arrays only on those surfaces of the artificial hand that might contact an object during grasp such as the palmar aspects of the digits and palm. However, if a bladder-like sensor system (e.g., [29], [41]) is implemented, the non-contact regions of the skin (radial or ulnar regions in this work) can provide a surprising wealth of information about finger-object contacts. While we and others have previously related electrode impedance data to contact forces [24], [26], [29], this work suggests that it may be useful to relate electrode impedance to skin deformation. For instance, compression of skin against the rigid core can occur even when a compressive force is not applied directly to that region of the skin because shear forces elsewhere can deform the continuous skin.

4.5 Moving Beyond Tactile Images Generated by Static Contact with Objects

The standard robotics approach to tactile sensing of shapes and edges is to create a "tactile image" (e.g., [19], [20], [21], [22]) from a series of static contacts with an object. As such, tactile sensor designs have often focused on achieving fine spatial resolution so that accurate reconstructions of images can be built through static contacts alone [45]. The tactile image approach could be useful for situations in which dynamic fingertip motions are not possible or desired. For instance, once an action has been planned and the static grasp of a tool has been established, only the tactile images from each fingertip would be available for haptically inferring the orientation of the tool within the hand or the stability of the grasp. Interestingly, we purposely degraded the spatial resolution of our tactile sensor data by clustering electrodes in order to reduce model complexity (Fig. 4). The performance of the SVR models (Table 2) suggests that spatial resolution is important, but that fine spatial resolution may not be essential for haptic exploration of edges.

The scope of the work presented here is the exploration of an unseen, unstructured environment in order to plan a grasp or manipulative action. For this exploratory scenario, dynamic approaches for collecting and processing tactile data seem better suited for perception than static approaches. Despite the fact that biological fingertips have fine spatial resolution capabilities [30], humans elect to use dynamic fingertip motions when identifying local features such as edges [13], [23]. Consider an example such as identifying the edge of your cellphone in your pocket. It is nearly impossible to force oneself to perform this task using a series of static contacts alone. While the completion of the task may be successful with static contacts, confirmation of edge orientation via contour-following is somehow more satisfying.

4.6 Generalizability of Proposed Approach to Naturalistic Conditions

The goal of this study was to use an artificial finger to estimate the orientation of an edge with respect to the fingertip's reference frame. In order to assess the feasibility of haptic perception of an edge, we controlled experimental variables such as contact force, angle, and speed, as well as stimulus width, compliance, and texture. Now that a baseline of SVR model performance has been established, additional experiments can be conceived to relax the constraints of this structured study and expand the approach to more naturalistic conditions. For instance, an artificial fingertip could be mounted to a prosthetic socket such that the fingertip contact conditions and trajectory could be controlled by an amputee instead of a robot. One could then assess the robustness of the SVR models to variations in contact force, stroke length, and stroke speed within a single EP motion as opposed to across trials. It will also be important to assess the effects of variations in initial fingertip contact on subsequent skin deformation, as addressed in Section 4.2. Although not discussed here, a recent study with foam and sponge stimuli led to promising results that edge orientation can also be estimated from haptic interactions with compliant stimuli using the methods presented here [46].

In practice, a human would not perform a series of EPs, store the resulting tactile signals, and then draw inferences on all tactile signals at the end. Rather, inferences would be drawn immediately after, if not during, the performance of an EP. Model performance could be used to rank the usefulness of different EPs such that a single EP could be selected based on the capabilities of the artificial hand and prior haptic information. For instance, one could implement a Bayesian exploration approach similar to that used for identification of surface texture [26] using the rankings from Table 2. An a priori estimate of edge orientation could be updated with haptic information gleaned from each subsequent EP until a user-defined confidence threshold had been reached.

The feasibility of real-time estimation of edge orientation should be assessed. Given that estimating edge orientation on 648 test trials took 4 sec, we hypothesize that it would take 6 ms to obtain an SVR model estimation from a single trial once input parameters had been extracted. Additional delays for input parameter extraction would depend on the specific model and whether computationally expensive techniques such as HHT were used.

For the purposes of a more advanced behavior such as contour-following or raster-like scanning of the fingertip [23], it may be necessary to develop models in which the fingertip trajectory length is shorter. Such an approach might enable frequent directional changes to the fingertip trajectory in order to follow curvatures in 3D. It may also be necessary to build a library of haptic experiences with vertices for contour-following of shapes with corners [47].

5 Conclusion

A tight relationship between voluntary actions and perception of tactile stimuli exists before, during, and after an action has been made. Psychophysics literature has

shown that perception drives action. That is, the property to be perceived drives the selection of an exploratory procedure based on the efficiency and accuracy of the EP for extracting information about the property of interest [13]. It stands to reason that, once an exploratory procedure has been performed, action should drive perception. In this work, we placed an emphasis on efficient processing and interpretation of tactile data as a function of the exploratory procedure. For example, if a static contact EP has been performed, it may not be fruitful to process and interpret fast tactile signals. Given the use of dynamic EPs, we elected to use information from multiple windows of the contact period. In this way, both spatial and temporal changes in tactile signals were used for perception of finger-object contact as opposed to a single, static tactile image. Further investigation of non-traditional tactile sensing and processing approaches could provide new insights into the haptic interactions between prosthetic hands and their environment.

Our work on the haptic exploration of edges could benefit the amputee community by enabling perception through the sense of touch. Establishing the orientation of a salient feature of an object with respect to the hand would be useful for building an internal model of an unseen object and planning the grasp and manipulation of the object. It remains unclear whether raw tactile signals or high-level abstractions of tactile signals should be made perceptible to amputees, and how many sensations can be effectively interpreted by an amputee simultaneously [48]. In the former approach, amputees would need to learn patterns of low-level signals in order to build internal models of stimuli and make inferences on physical interactions with the environment. Our work suggests that skin deformation of a compliant fingerpad could serve as a rich source of low-level tactile signals. Alternatively, high-level abstractions of tactile signals could be provided to subjects, just as grip force can be conveyed through tactors to upper-limb amputees [48] and navigational cues can be conveyed through haptic vests [49] and belts [50] to the blind. Edge orientation with respect to the fingertip could be conveyed using direct stimulation of the nervous system or tactile shape displays [51] and could be used to plan a reorientation of the limb or a preshaping of a grasp. Also, internal models of objects could be developed to enable a prosthetic or robotic hand to perform low-level fingertip adjustments semi-autonomously, thereby allowing the user to concentrate on high-level aspects of the task. Whether low-level or high-level in nature, tactile feedback would enable amputees to build action-perception relationships that are currently limited to use of visual feedback and proprioceptive feedback from residual limbs.

Acknowledgments

The authors wish to thank Ismael Reveles for assistance with data collection and literature review, Dr. Stephen Helms Tillery for suggestions on the data collection protocol, and Dr. Ehsan T. Esfahani for recommending the Hilbert-Huang Transform technique. This work was supported in part by the US National Science Foundation under Grants #0932389, #0954254, and #1208519.

References

[1] C. Cipriani, C. Antfolk, C. Balkenius, B. Rosen, G. Lundborg, M.C. Carrozza, and F. Sebelius, "A Novel Concept for a Prosthetic Hand with a Bidirectional Interface: A Feasibility Study," *IEEE Trans. Biomedical Eng.*, vol. 56, no. 11, pp. 2739-2743, Nov. 2009.

[2] A.E. Schultz, P.D. Marasco, and T.A. Kuiken, "Vibrotactile Detection Thresholds for Chest Skin of Amputees Following Targeted Reinnervation Surgery," *Brain Research*, vol. 1251, no. 11, pp. 121-129, Jan. 2009.

[3] G.S. Dhillon and K.W. Horch, "Direct Neural Sensory Feedback and Control of a Prosthetic Arm," *IEEE Trans. Neural Systems and Rehabilitation Eng.*, vol. 13, no. 4, pp. 468-472, Dec. 2005.

[4] R. Romo, A. Hernández, A. Zainos, and E. Salinas, "Somatosensory Discrimination Based on Cortical Microstimulation," *Nature*, vol. 392, no. 6674, pp. 387-390, Mar. 1998.

[5] J.E. O'Doherty, M.A. Lebedev, P.J. Ifft, K.Z. Zhuang, S. Shokur, H. Bleuler, and M.A.L. Nicolelis, "Active Tactile Exploration Using a Brain-Machine-Brain Interface," *Nature*, vol. 479, pp. 228-231, Nov. 2011.

[6] C. Overstreet, J.D. Klein, and S. Helms Tillery, "Excitation of Distinct Pools of Somatosensory Neurons Via Intracortical Microstimulation," *Proc. 42nd Ann. Meeting Soc. Neuroscience*, 2013.

[7] J.T. Belter and A.M. Dollar, "Performance Characteristics of Anthropomorphic Prosthetic Hands," *Proc. IEEE Int'l Conf. Rehabilitation Robotics*, pp. 1-7, 2011.

[8] M. Siegel, "The Sense-Think-Act Paradigm Revisited," *Proc. First Int'l Workshop Robotic Sensing (ROSE '03)*, p. 5, 2003.

[9] M.T. Ciocarlie and P.K. Allen, "On-Line Interactive Dexterous Grasping," *Proc. Sixth Int'l Conf. Haptics: Perception, Devices and Scenarios*, pp. 104-113, 2008.

[10] A.T. Miller and P.K. Allen, "GraspIt! A Versatile Simulator for Robotic Grasping," *IEEE Robotics & Automation Magazine*, vol. 11, no. 4, pp. 110-122, Dec. 2004.

[11] D.J. Atkins, D.C.Y. Heard, and W.H. Donovan, "Epidemiologic Overview of Lndividuals with Upper-Limb Loss and Their Reported Research Priorities," *J. Prosthetics and Orthotics*, vol. 8, no. 1, pp. 2-11, 1996.

[12] M.A. Plaisier, W.M. Bergmann Tiest, and A.M.L. Kappers, "Salient Features in 3-D Haptic Shape Perception," *Attention, Perception, & Psychophysics*, vol. 71, no. 2, pp. 421-430, 2009.

[13] S.J. Lederman and R.L. Klatzky, "Hand Movements: A Window into Haptic Object Recognition," *Cognitive Psychology*, vol. 19, no. 3, pp. 342-368, July 1987.

[14] S.J. Lederman and R.L. Klatzky, "Relative Availability of Surface and Object Properties during Early Haptic Processing," *J. Experimental Psychology: Human Perception and Performance*, vol. 23, no. 6, pp. 1680-1707, Dec. 1997.

[15] B. Massa, S. Roccella, M.C. Carrozza, and P. Dario, "Design and Development of an Underactuated Prosthetic Hand," *Proc. IEEE Int'l Conf. Robotics and Automation (ICRA'02)*, vol. 4, pp. 3374-3379, 2002.

[16] R.R. Ma, L.U. Odhner, and A.M. Dollar, "A Modular, Open-Source 3D Printed Underactuated Hand," *Proc. Int'l Conf. Robotics and Automation*, 2013.

[17] J. Baeten, W. Verdonck, H. Bruyninckx, and J. De Schutter, "Combining Force Control and Visual Servoing for Planar Contour Following," *Int'l J. Machine Intelligence and Robotic Control*, vol. 2, no. 2, pp. 69-75, 2000.

[18] H. Koch, A. Konig, A. Weigl-Seitz, K. Kleinmann, and J. Suchy, "Multisensor Contour Following with Vision, Force, and Acceleration Sensors for an Industrial Robot," *IEEE Trans. Instrumentation and Measurement*, vol. 62, no. 2, pp. 268-280, Feb. 2013.

[19] A.D. Berger and P.K. Khosla, "Using Tactile Data for Real-Time Feedback," *Int'l J. Robotics Research*, vol. 10, no. 2, pp. 88-102, Apr. 1991.

[20] E.M. Petriu, W.S. McMath, S.S.K. Yeung, and N. Trif, "Active Tactile Perception of Object Surface Geometric Profiles," *IEEE Trans. Instrumentation and Measurement*, vol. 41, no. 1, pp. 87-92, Feb. 1992.

[21] T. Mei, W.J. Li, Y. Ge, Y. Chen, L. Ni, and M.H. Chan, "An Integrated MEMS Three-Dimensional Tactile Sensor with Large Force Range," *Sensors and Actuators A: Physical*, vol. 80, no. 2, pp. 155-162, 2000.
[22] H.-K. Lee, S.-I. Chang, and E. Yoon, "A Flexible Polymer Tactile Sensor: Fabrication and Modular Expandability for Large Area Deployment," *J. Microelectromechanical Systems*, vol. 15, no. 6, pp. 1681-1686, Dec. 2006.
[23] K. Huynh, C.E. Stepp, L.W. White, J.E. Colgate, and Y. Matsuoka, "Finding a Feature on a 3D Object through Single-Digit Haptic Exploration," *Proc. IEEE Haptics Symp.*, pp. 83-89, 2010.
[24] C.H. Lin, T.W. Erickson, J.A. Fishel, N. Wettels, and G.E. Loeb, "Signal Processing and Fabrication of a Biomimetic Tactile Sensor Array with Thermal, Force and Microvibration Modalities," *Proc. IEEE Int'l Conf. Robotics and Biomimetics*, pp. 129-134, 2009.
[25] Z. Su, J.A. Fishel, T. Yamamoto, and G.E. Loeb, "Use of Tactile Feedback to Control Exploratory Movements to Characterize Object Compliance," *Frontiers in Neurorobotics*, vol. 6, 2012.
[26] J.A. Fishel and G.E. Loeb, "Bayesian Exploration for Intelligent Identification of Textures," *Frontiers in Neurorobotics*, vol. 6, p. 4, 2012.
[27] V. Chu, I. McMahon, L. Riano, C.G. McDonald, Q. He, J.M. Perez-Tejada, M. Arrigo, N. Fitter, J.C. Nappo, T. Darrell, and K.J. Kuchenbecker, "Using Robotic Exploratory Procedures to Learn the Meaning of Haptic Adjectives," *Proc. IEEE Int'l Conf. Robotics and Automation*, pp. 3033-3040, 2013.
[28] D. Xu, G.E. Loeb, and J.A. Fishel, "Tactile Identification of Objects Using Bayesian Exploration," *Proc. IEEE Int'l Conf. Robotics and Automation*, 2013.
[29] N. Wettels, V.J. Santos, R.S. Johansson, and G.E. Loeb, "Biomimetic Tactile Sensor Array," *Advanced Robotics*, vol. 22, pp. 829-849, Aug. 2008.
[30] R.S. Johansson and J.R. Flanagan, "Coding and Use of Tactile Signals from the Fingertips in Object Manipulation Tasks," *Nature Rev. Neuroscience*, vol. 10, pp. 345-359, 2009.
[31] J. Fishel, G. Lin, and G.E. Loeb, "SynTouch LLC BioTac Product Manual, v.16," Feb. 2013.
[32] J. Fishel and G.E. Loeb, "Sensing Tactile Microvibrations with the BioTac—Comparison with Human Sensitivity," *Proc. IEEE RAS / EMBS Int'l Conf. Biomedical Robotics and Biomechatronics,* Roma, Italy, pp. 1122-1127, 2012.
[33] S.J. Bensmaia, P.V. Denchev, J.F. Dammann, J.C. Craig, and S.S. Hsiao, "The Representation of Stimulus Orientation in the Early Stages of Somatosensory Processing," *J. Neuroscience*, vol. 28, no. 3, pp. 776-786, Jan. 2008.
[34] S.J. Bensmaia, S.S. Hsiao, P.V. Denchev, J.H. Killebrew, and J.C. Craig, "The Tactile Perception of Stimulus Orientation," *Somatosensory & Motor Research*, vol. 25, no. 1, pp. 49-59, 2008.
[35] N.E. Huang, Z. Shen, S.R. Long, M.C. Wu, H.H. Shih, Q. Zheng, N.-C. Yen, C.C. Tung, and H.H. Liu, "The Empirical Mode Decomposition and the Hilbert Spectrum for Nonlinear and Non-Stationary Time Series Analysis," *Proc. Royal Soc. of London A*, vol. 454, no. 1971, pp. 903-995, Mar. 1998.
[36] N.E. Huang, "Introduction to the Hilbert-Huang Transform and Its Related Mathematical Problems," *Interdisciplinary Math.*, vol. 5, pp. 1-26, 2005.
[37] D. Donnelly, "The Fast Fourier and Hilbert-Huang Transforms: A Comparison," *Int'l J. Computers, Comm. & Control*, vol. 1, no. 4, pp. 45-52, 2006.
[38] W. Liu, Y. Yan, and R. Wang, "Application of Hilbert-Huang Transform and SVM to Coal Gangue Interface Detection," *J. Computers*, vol. 6, no. 6, pp. 1262-1269, June 2011.
[39] P.-N. Tan, M. Steinbach, and V. Kumar, *Introduction to Data Mining*. Pearson Addison Wesley, 2006.
[40] M. Hall, E. Frank, G. Holmes, B. Pfahringer, P. Reutemann, and I.H. Witten, "The WEKA Data Mining Software: An Update," *ACM SIGKDD Explorations Newsletter*, vol. 11, no. 1, pp. 10-18, 2009.
[41] D. Hristu, N. Ferrier, and R.W. Brockett, "The Performance of a Deformable-Membrane Tactile Sensor: Basic Results on Geometrically-Defined Tasks," *Proc. IEEE Int'l Conf. Robotics and Automation*, vol. 1, pp. 508-513, 2000.
[42] G. De Maria, C. Natale, and S. Pirozzi, "Force/Tactile Sensor for Robotic Applications," *Sensors and Actuators A: Physical*, vol. 175, pp. 60-72, Mar. 2012.
[43] R.D. Ponce Wong, J.D. Posner, and V.J. Santos, "Flexible Microfluidic Normal Force Sensor Skin for Tactile Feedback," *Sensors and Actuators A: Physical*, vol. 179, pp. 62-69, June 2012.
[44] D. Prattichizzo and J.C. Trinkle, "Grasping," *Springer Handbook of Robotics*, B. Siciliano, and O. Khatib, eds., pp. 671-700, Springer-Verlag, 2008.
[45] R. Dahiya, G. Metta, M. Valle, and G. Sandini, "Tactile Sensing—From Humans to Humanoids," *IEEE Trans. Robotics*, vol. 26, no. 1, pp. 1-20, Feb. 2010.
[46] R.D. Ponce Wong, "Towards Haptic Intelligence for Artificial Hands: Development and Use of Deformable, Fluidic Tactile Sensors to Relate Action and Perception," PhD dissertation, Arizona State University, Tempe, AZ, 2013.
[47] J. Baeten and J. De Schutter, "Hybrid Vision/Force Control at Corners in Planar Robotic-Contour Following," *IEEE /ASME Trans. Mechatronics*, vol. 7, no. 2, pp. 143-151, June 2002.
[48] K. Kim and E. Colgate, "Haptic Feedback Enhances Grip Force Control of sEMG-ControlledProsthetic Hands in Targeted Reinnervation Amputees," *IEEE Trans. Neural Systems and Rehabilititation Eng.*, vol. 20, no. 6, pp. 798-805, Nov. 2012.
[49] L.A. Jones, M. Nakamura, and B. Lockyer, "Development of a Tactile Vest," *Proc. 12th Int'l Symp. Haptic Interfaces for Virtual Environment and Teleoperator Systems (HAPTICS '04)*, pp. 82-89, 2004.
[50] T. McDaniel, S. Krishna, V. Balasubramanian, D. Colbry, and S. Panchanathan, "Using a Haptic Belt to Convey Non-Verbal Communication Cues during Social Interactions to Individuals Who Are Blind," *Proc. IEEE Int'l Workshop Haptic Audio Visual Environments and Games (HAVE '08)*, pp. 13-18, 2008.
[51] C.R. Wagner, S.J. Lederman, and R.D. Howe, "Design and Performance of a Tactile Shape Display Using RC Servomotors," *Electronic J. Haptics Research*, vol. 3, no. 4, 2004.

Ruben D. Ponce Wong received the BS degree in bioengineering in 2008 and the MS and PhD degrees in mechanical engineering in 2013 from Arizona State University. His research interests include the fabrication of microfluidic tactile sensors and employment of machine learning algorithms on multimodal tactile sensor data for haptic exploration and robot control. He is a member of the IEEE.

Randall B. Hellman received the BS degree in mechanical engineering from Purdue University in 2008. Upon graduation, he was at Kiewit Energy as a field engineer. Since 2011, he has been a doctoral student in mechanical engineering at Arizona State University. His research interests include robotic hands, tendon driven systems, motion planning, and haptic exploration. He is a student member of the IEEE.

Veronica J. Santos received the BS degree in mechanical engineering with a music minor from the University of California at Berkeley in 1999, and the MS and PhD degrees in mechanical engineering with a biometry minor from Cornell University in 2004 and 2007, respectively. From 2007 to 2008, she was a postdoctoral research associate at the Mann Institute for Biomedical Engineering at the University of Southern California. She is currently an assistant professor of mechanical and aerospace engineering at Arizona State University. She received the 2010 NSF CAREER award and was selected to participate in the 2010 National Academy of Engineering Frontiers of Engineering Education Symposium. Her research interests include hand biomechanics, neural control of movement, robotics, prosthetics, and tactile sensors. She is a member of the IEEE, IEEE Engineering and Medicine in Biology Society and IEEE Robotics and Automation Society.